Research Article

Kanagasabapathy Sivasubramanian*, Shanmugam Sabarinathan, Moorthy Muruganandham, Palanivel Velmurugan, Natarajan Arumugam, Abdulrahman I. Almansour, Raju Suresh Kumar, and Subpiramaniyam Sivakumar*

Antioxidant, antibacterial, and cytotoxicity potential of synthesized silver nanoparticles from the *Cassia alata* leaf aqueous extract

https://doi.org/10.1515/gps-2023-0018
received January 29, 2023; accepted March 29, 2023

Abstract: The current research focuses on the silver nanoparticles (AgNPs) synthesis from the *Cassia alata* aqueous leaf extract. Various production parameters like pH (4, 5, 6, 7, 8, 9, and 10), metal ion concentration (1, 2, 3, 4, and 5 mM), and substrate (leaf extract) concentration (0.5, 1, 1.5, 2 and 2.5 mL) were optimized. UV-visible spectroscopy was used to identify the production by scanning the wavelength from 200 to 800 nm. Visual color change from light green to brown was designated as prior confirmation of the AgNP production. Physical characterization of AgNPs was carried out using scanning electron microscopy, Fourier-transform infrared spectroscopy, X-ray energy-dispersive spectroscopy, and X-ray diffraction. Furthermore, the obtained AgNPs show significant antibacterial activity for *Staphylococcus aureus*, *Pseudomonas* sp. *Klebsiella* sp., *Proteus* sp., and *Enterobacter* sp. The antioxidant potential was determined by α,α-diphenyl-β-picrylhydrazyl assay and cytotoxicity by (3-(4,5-dimethylthiazol-2-yl)-2,5-diphenyltetrazolium bromide) tetrazolium reduction assay on human lung cancer cell lines (A549). AgNPs confirmed potent antibacterial activity against skin infections, demonstrating their medicinal significance and are therefore crucial for creating a medicinal formulation with antibacterial properties.

Keywords: green synthesis, *Cassia alata*, AgNPs, characterization, antibacterial activity

*** Corresponding author: Kanagasabapathy Sivasubramanian,** Department of Microbiology, Sri Sankara Arts and Science College, Kanchipuram, Tamil Nadu, India; Centre for Materials Engineering and Regenerative Medicine, Bharath Institute of Higher Education and Research, Selaiyur, Chennai, Tamil Nadu 600126, India, e-mail: skssmani2018@gmail.com
*** Corresponding author: Subpiramaniyam Sivakumar,** Department of Bioenvironmental Energy, College of Natural Resource and Life Sciences, Pusan National University, Miryang-si, Gyeongsangnam-do 50463, Republic of Korea, e-mail: ssivaphd@yahoo.com
Shanmugam Sabarinathan: Department of Microbiology, Sri Sankara Arts and Science College, Kanchipuram, Tamil Nadu, India
Moorthy Muruganandham, Palanivel Velmurugan: Centre for Materials Engineering and Regenerative Medicine, Bharath Institute of Higher Education and Research, Selaiyur, Chennai, Tamil Nadu 600126, India
Natarajan Arumugam, Abdulrahman I. Almansour, Raju Suresh Kumar: Department of Chemistry, College of Science, King Saud University, P.O. Box 2455, Riyadh 11451, Saudi Arabia

1 Introduction

Nanotechnology is a combination of nanoscience, engineering, and technology, as well as physics, chemistry, and biology. Silver nanoparticles (AgNPs) inhibit and inactivate microorganisms [1]. Ionic silver and silver-derived compounds are recognized to be lethal to microbes and are employed as antibacterial agents [2–4]. Plants can produce nanoparticles without the need for microbial cell cultures. Silver dressings, silver nitrate, silver zeolite, and AgNPs are antibacterial substances that have been extensively researched [5]. AgNPs produced from plants and biological sources have exceptional properties in nonlinear optics, intersperse materials for batteries, optical receptors, chemical reaction catalysts, bio-labeling, and antimicrobial capabilities [6,7]. Plant-mediated nanoparticle production is easy and fast. For self-assembly and physiochemical characteristics, size and shape must be considered in the preparation of AgNPs [8]. Silver and AgNPs are most important in medicine, such as in topical ointments, to prevent burn and wound infections [9]. Silver has long inhibited microorganisms in medicinal and industrial processes. The current physicochemical procedures produce toxic by-products; hence, there is an increasing need for ecologically friendly nanomaterial synthesis protocols [10]. Biological synthesis technologies

allow "green" nanoparticle creation and improved crystal growth and stabilization. This has accelerated research on synthesis directions that increase form and size control for nanotechnological applications. Synthesizing AgNPs from ecologically friendly sources like plant extract has many advantages in pharmacological and biological applications.

C. alata (synonym: *Senna alata*) is a Leguminosae subfamily Fabaceae plant used in traditional medicine. This plant's roots, leaves, and blossoms are antibacterial, antifungal, antitumor, expectorant, and useful in treating urinary tract issues, asthma, bronchitis, constipation, anti-malarial, asthmatic, diabetic, ringworm, snakebite, scorpion bite, skin illnesses, impetigo, syphilis sores, itching, mycosis, herpes, and eczema [11,12]. In addition, *C. alata* has been reported to have potential anti-allergic, anti-inflammatory, antioxidant, anticancer, antidiabetic, and antifungal properties. Qualitative testing determined the following phytochemicals in *Cassia* sp. aqueous leaf extract: flavones, flavonols, flavonoid glycosides, tannins, phlobatanins, β-sitosterol-β-D-glucoside, alkaloids, sugars, glycosides, saponins, phenolics, proteins, and amino acids [12,13]. Several studies report only the antibacterial and antioxidant properties of the synthesized AgNPs from *C. alata*, and no report has been recorded against the cancer cells. Hence, the present study was designed to evaluate synthesized AgNPs using the aqueous leaf extract from *C. alata* for their biologically active compounds that have pharmacologically significant therapeutic properties such as antioxidant, free radical scavenging, and anticancer properties. Since AgNPs are essential for plant eco-friendly synthesis and have strong chemical stability and favorable interactions with plant metabolites, these factors led to the selection of AgNPs.

2 Materials and methods

2.1 Chemical and media

All the solvents and chemicals used were of analytical grade and were obtained from SRL India. Microbiological media was obtained from Hi-media (Mumbai, India). Tetracycline was used as the reference antibiotics.

2.2 Collection and preparation of aqueous leaf extract

Healthy and matured leaf samples of *C. alata* were collected in and around Enathur village (latitude, 12.84°N; longitude, 79.73°E) in Kanchipuram, Tamil Nadu, India, in January 2022. All the samples were identified using the morphological characters encrypted in the monograph. The *C. alata* leaves were cut into small pieces using sterile scissors, followed by washing. About 50 g of leaves were soaked in 100 mL of distilled water and boiled in a 500 mL beaker to extract the phytoconstituents using a heating mantle for 30 min at 100°C. Later, the extract was cooled and filtered. This extract is freshly prepared for each experiment.

2.3 Phytochemical screening of *C. alata* leaf extracts

The extracts were screened for phytochemical content to detect the presence of flavonoids, phenols, cardiac glycosides, terpenoids, glycosides, anthraquinones, and quinones. The mixture contained 1 mL of extract, 2 mL of distilled water, and a few drops of 10% aqueous $FeCl_3$. The presence of flavonoids is indicated by the presence of a brown color, whereas the presence of phenols is indicated by the presence of a blue or green color. After combining 5 mL of the extract, 2 mL of chloroform, and 3 mL of strong sulfuric acid, a reddish-brown color at the interface indicated the presence of terpenoids. After combining 1 mL of the extract with 1 mL of glacial acetic acid, the mixture was allowed to cool before adding 2–3 drops of ferric chloride. Then 2 mL of concentrated H_2SO_4 was added. The presence of glycosides can be identified at the point where two layers meet by the formation of a reddish-brown ring. Following the addition of 2 mL of hydrochloric acid to 1 mL of the extract, the resulting liquid was heated in a water bath for 15 min before cooling and filtering. After treating the filtrate with a 10% solution of potassium hydroxide, the aqueous layer turned pinkish-red, indicating the presence of anthraquinones. Chloroform was added to the filtrate. A red tint was produced after adding 1 mL of strong sulfuric acid to 1 mL of extract, indicating the presence of quinones [14].

2.4 Production optimization of AgNPs

To synthesize AgNPs, 1 mL of 0.1 mM silver nitrate solution and 9 mL of *C. alata* aqueous leaf extract were thoroughly mixed at room temperature. By using a UV-visible (UV-Vis) spectrophotometer to measure the absorption spectra in the 200–800 nm region, the bio-reduction of

silver ions in the solution was periodically monitored. The pH was changed to 4, 5, 6, 7, 8, 9, and 10 by adding 1.0 mL of the extract and 9.0 mL of 0.1 mM silver nitrate to maximize the pH. To find the ideal concentration, a wavelength scan was performed with the metal ion concentrations set to 1, 2, 3, 4, and 5 mM at pH 9.0. To check the ideal extract concentration for the formation of AgNPs, extracts of 0.5, 1, 1.5, 2, and 2.5 mL were utilized with the ideal pH and metal ion concentration. AgNPs were produced in large quantities under ideal circumstances. Following mass production, AgNPs were purified by repetitively centrifuging at 12,000 rpm for 30 min. The pellet was employed for characterization after being dried in a hot air oven [15,16].

2.5 Characterization of synthesized AgNPs

A UV-Vis spectrophotometer was used to characterize the bio-reduced AgNPs that were synthesized, and the results were based on an investigation of the pH, substrate, and silver nitrate concentrations at wavelengths between 200 and 800 nm [14]. The biomolecules of the synthesized AgNPs using the aqueous leaf extract of *C. alata* were identified by Fourier transform infrared (FTIR) spectroscopy. The 500–4,000 cm^{-1} range of the spectrum was used to capture the FTIR. A distinct functional group might be identified by cataloging and categorizing the many vibrational modes that were seen in AgNPs [15]. Transmission electron microscopy (TEM), utilizing a JEOL JEM-2100 at a 200 kV acceleration voltage, was used to determine the size and shape of AgNPs. The elemental composition of the synthesized AgNPs was determined using an energy-dispersive X-ray spectroscopy (EDX) spectrum. The analysis of X-ray diffraction (XRD) patterns revealed the crystalline nature as well as the size and phase identification of the green AgNPs produced from the *C. alata* leaf extract [17].

2.6 Antibacterial activity of AgNPs

To evaluate the antibacterial activity of AgNPs, the disk diffusion method was employed with slight modification. Bacterial pathogens, including *Staphylococcus aureus*, *Pseudomonas* sp., *Klebsiella* sp., *Proteus* sp., and *Enterobacter* sp., were grown in the Muller–Hinton broth (MHB) overnight at 37°C and adjusted to 0.5 McFarland standards. All of the bacterial strains mentioned above were obtained from the Department of Microbiology at Sri Sankara Arts and Science College in Enathur, Kanchipuram. Each pathogenic strain was plated in sterile environments using the spread method, and 0.1 mL of Muller–Hinton agar. In the sterile empty disk, the synthesized AgNPs were loaded in different concentrations (50 and 100 µL). The sterile disk was loaded with the same concentration of aqueous leaf extract. Using forceps, the disk was gently placed in the culture plates. The plates were incubated for 24 h at 37°C, and the zone of inhibition was measured after the incubation period [18].

2.7 Minimum inhibitory concentration (MIC)

The minimum concentration (MIC) of the synthesized AgNPs and leaf extract was calculated by measuring the quantity necessary to inhibit the growth of the tested pathogens. To determine the MIC, 96-well microtiter plates were utilized. Initially, the MHB with different concentrations of AgNPs and leaf extracts ranging from 0 to 5 $mg{\cdot}mL^{-1}$ were prepared. The MHB well and antibiotic control were then injected with the test pathogens (10^7 $CFU{\cdot}mL^{-1}$) at a volume of 100 $\mu g{\cdot}mL^{-1}$. The test was run in triplicate, and the outcomes were observed after a 24 h incubation period at 37°C [19].

2.8 Antioxidant activity

The α,α-diphenyl-β-picrylhydrazyl (DPPH) free radical scavenging capability of AgNPs and the aqueous leaf extract was investigated using a modified version of the usual approach [20]. Just before the experiment, DPPH (0.1 M), AgNPs (25–400 $\mu g{\cdot}mL^{-1}$), and the aqueous leaf extract (25–400 $\mu g{\cdot}mL^{-1}$) were dissolved in methanol. About 1 mL of each concentration was combined with 1 mL of DPPH in a separate test tube. The prepared test tubes were then incubated for 30 min in the dark. A total of 200 µL of the reaction mixture was removed from each test tube and placed into a 96-well microtiter plate as the last step. The absorbance was measured at 517 nm using a multi-leader. AgNPs and the aqueous leaf extract were used in this triplicate test. The negative and positive controls were DPPH and ascorbic acid, respectively. Methanol was used as a blank for the experiment at the same time. The activity of radical scavenging was computed as follows:

$$\text{Free radical scavenging activity (\%)} = \frac{\text{Control Abs} - \text{Test sample (Abs)}}{\text{Control (Abs)}} \times 100 \quad (1)$$

2.9 *In vitro* cytotoxicity studies

The (3-(4,5-dimethylthiazol-2-yl)-2,5-diphenyltetrazolium bromide) tetrazolium reduction (MTT) assay is a non-radioactive colorimetric assay that measures cytotoxicity and the number of live cells by observing the increase in the tetrazolium salt metabolism. After seeding lung cancer cells (A549) into 96-well plates at a density of 1×10^6 cells·mL^{-1}, the plates were placed in an incubator for 24 h. Following that, the cells were exposed to a range of drug formulation doses ranging from 25 to 400 µg·mL^{-1}. The cells were then kept at 37°C for 24 h while being exposed to 5% carbon dioxide. Following incubation, 0.5 mg·mL^{-1} MTT was applied to the incubated cells. The cells were then cultured for another 4 h. Following incubation, 0.5 mg·mL^{-1} MTT was applied to the incubated cells. The cells were then cultured for another 4 h. Following that, 100 µL of dimethyl sulfoxide was added to each well, and the contents were thoroughly mixed. Additionally, cells were treated with doxorubicin (50 µg·mL^{-1} [100 µL·well^{-1}]) as a positive control and complete medium (100 µL·well^{-1}) as a negative control. A multimode reader was used to measure the absorbance at a wavelength of 570 nm [21].

2.10 Statistical analysis

All assays were carried out in triplicate on each occasion. The data were presented as mean ± standard deviation (SD) from three separate trials.

3 Results and discussion

3.1 Production and optimization of AgNPs

The presence of flavonoids, phenols, cardiac glycosides, terpenoids, glycosides, anthraquinones, and quinones (Table 1) was observed in the aqueous extract of *C. alata* leaf. A similar result was observed in the same plant, *C. alata*, which is one of the most important species of the genus Cassia, which is rich in anthraquinones and polyphenols. The leaves of *C. alata* have been qualitatively analyzed for the presence of primarily five pharmacologically active anthraquinones: rhein, aloe emodin, chrysophanol, emodin, and physcion, as well as the flavonoid, kaempferol [12]. The collection of *C. alata* leaves, extract preparation, and the production of AgNPs are shown in Figure 1.

Table 1: Phytochemical analysis of the *C. alata* leaf extract

Test	Results
Flavonoids	+
Phenols	+
Cardiac glycosides	+
Terpenoids	+
Glycosides	+
Anthraquinones	+
Quinones	+

As a result of the surface plasmon resonance phenomenon, the reduction of silver ions into AgNPs during exposure to plant extracts is followed by a gradual increase in color development from clear reddish brown. pH influences the synthesis of nanoparticles at various pH levels ranging from 2 to 10; the light green color changes into brown color when the pH increases. Stability and maximum synthesis of AgNPs were obtained at pH 9.0 (Figure 2a). To optimize the metal ions, various concentrations of $AgNO_3$ ranging from 100 to 500 mM were used for the synthesis of the nanoparticle. Among them, 0.3 M showed a maximum synthesis of AgNPs (Figure 2b), which is more similar to the findings of the previous study. Similarly, substrate concentrations were optimized by using the leaf extract at various levels ranging between 0.5 and 2.5 mL. High stability and maximum synthesis of nanoparticles were obtained at 2 mL with a dark brown color (Figure 2c) and the absorption peak at 460 nm indicated the biosynthesis of silver nanoparticles. The absorbance was measured between 300 and 800 nm wavelength using a UV-Vis spectrophotometer [22].

3.2 Characterization of the synthesized AgNPs

The UV-Vis spectra confirmed the reduction of AgNPs in the silver complex's aqueous solution during the reaction with *Cassia* sp. leaf extracts. After incubation, the maximum absorption of AgNPs was measured. The absorption of reddish-brown colloids was significant at 420 nm, indicating the presence of solitary spherical AgNPs. At wavelengths between 200 and 800 nm, the optical density was recorded, and the results were analyzed. To pinpoint the functional groups of the produced AgNPs and proteins that surround them as stabilizing agents, FTIR measurements were made on AgNPs, and the results reveal various bond strains at various peaks [23]. The synthesized AgNPs exhibited adsorption peaks at 845,

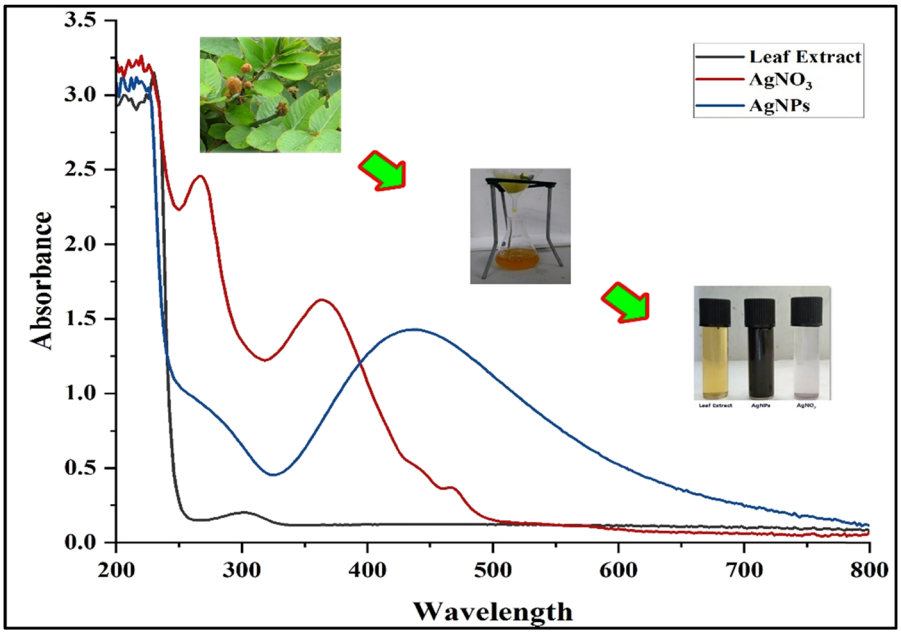

Figure 1: UV-Vis absorption spectra and color change (inset) for AgNP formation using the *C. alata* leaf extract.

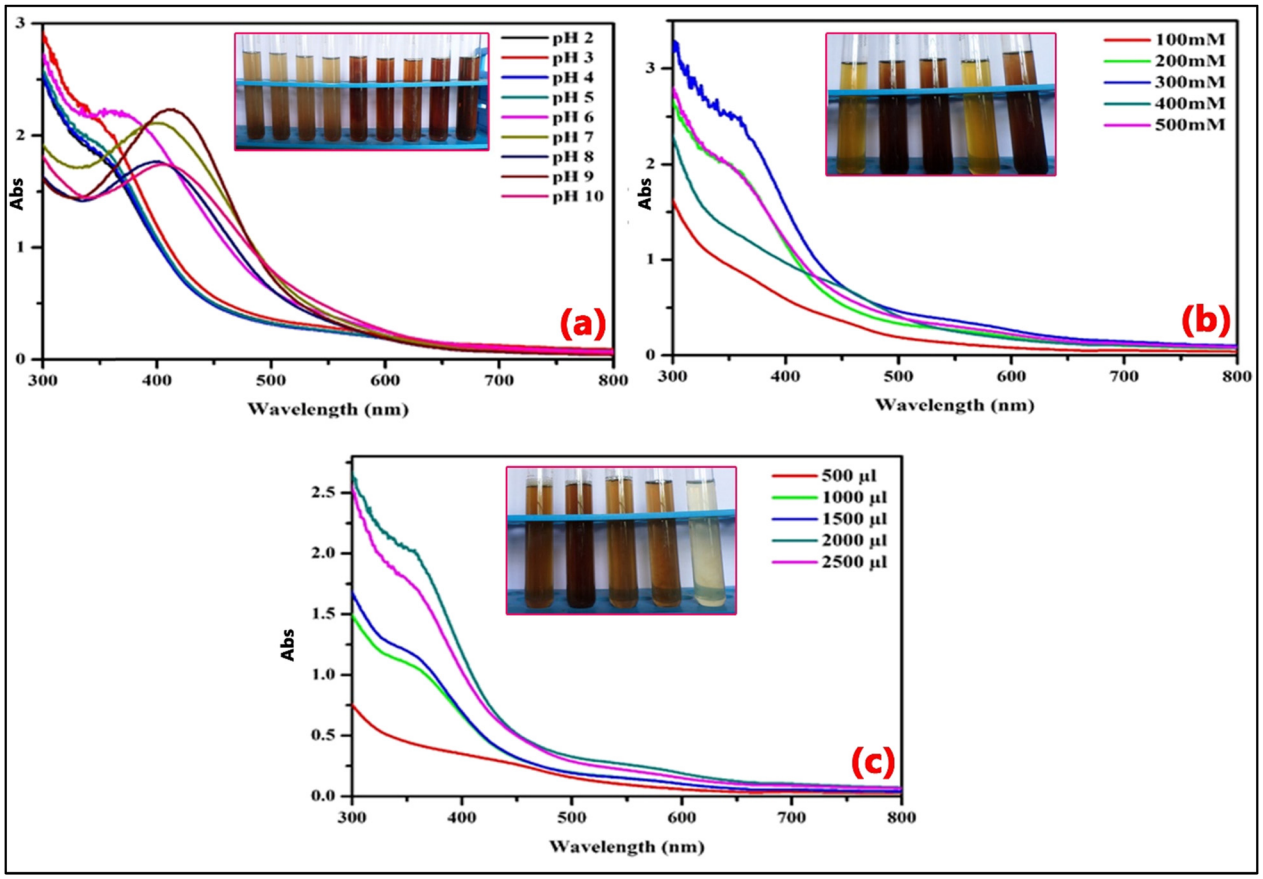

Figure 2: Effect of pH (a), metal ion concentration (b), and substrate concentration (c) on AgNP synthesis by *C. alata* leaf extract. The inset image shows the reaction.

1,008, 1,388, 1,635, and 3,465 cm^{-1} (Figure 3a). The band, which was visible at 3,465 cm^{-1}, was caused by H–OH stretching of phenols and the band's absorption was at 1,635 cm^{-1}. The C═O stretching of aldehydes and ketones is indicated by the absorption of the band at 1,635 cm^{-1}. The N═O bending of nitro groups correlates with the peak at 1,388 cm^{-1}. The C–O stretching of esters is represented by the band that was seen at 1,008 cm^{-1}. The 845 cm^{-1} peaks are caused by the C–H stretching of alkenes. Additionally, the reduction of silver metal ions to AgNPs is initiated by the redox reaction of the reducing sugar molecules [24].

The high-density AgNPs synthesized from *C. alata*, as seen in the TEM image (Figure 3b), supported the emergence of the silver nanostructure. The scanning electron microscopy images of AgNPs revealed that they are evenly distributed in solution, 20 nm in size, and spherically formed. The EDX spectrum displays (Figure 3c) peaks that correspond to the constituent parts of the sample itself [25]. The presence of silver is confirmed by the elemental profile of produced nanoparticles, which displays the largest X-ray energy peak at 3 keV due to silver. XRD examination also supported that the green AgNPs produced from the *C. alata* leaf extract were crystal-like and represented the XRD pattern obtained for AgNPs that were produced utilizing the *C. alata* aqueous leaf extract. The size, phase, and crystal structure of AgNPs were all determined by the XRD examination [26]. It displayed strong and distinct peaks at 2θ = 32.05°, 37.96°, 46.27°, 55.25°, 57.39°, and 68.51°. The XRD pattern revealed four diffraction peaks that may be indexed to the 111, 200, 220, and 311 planes of the face-centered cubic crystalline silver, respectively, at 32.05°, 46.27°, 55.25°, and 57.39° [27]. By calculating the full width at half-maximum of the Bragg reflection corresponding to the (111) crystalline plane of AgNPs, the average size of AgNPs was estimated using the Debye–Schreyer equation (Figure 3d).

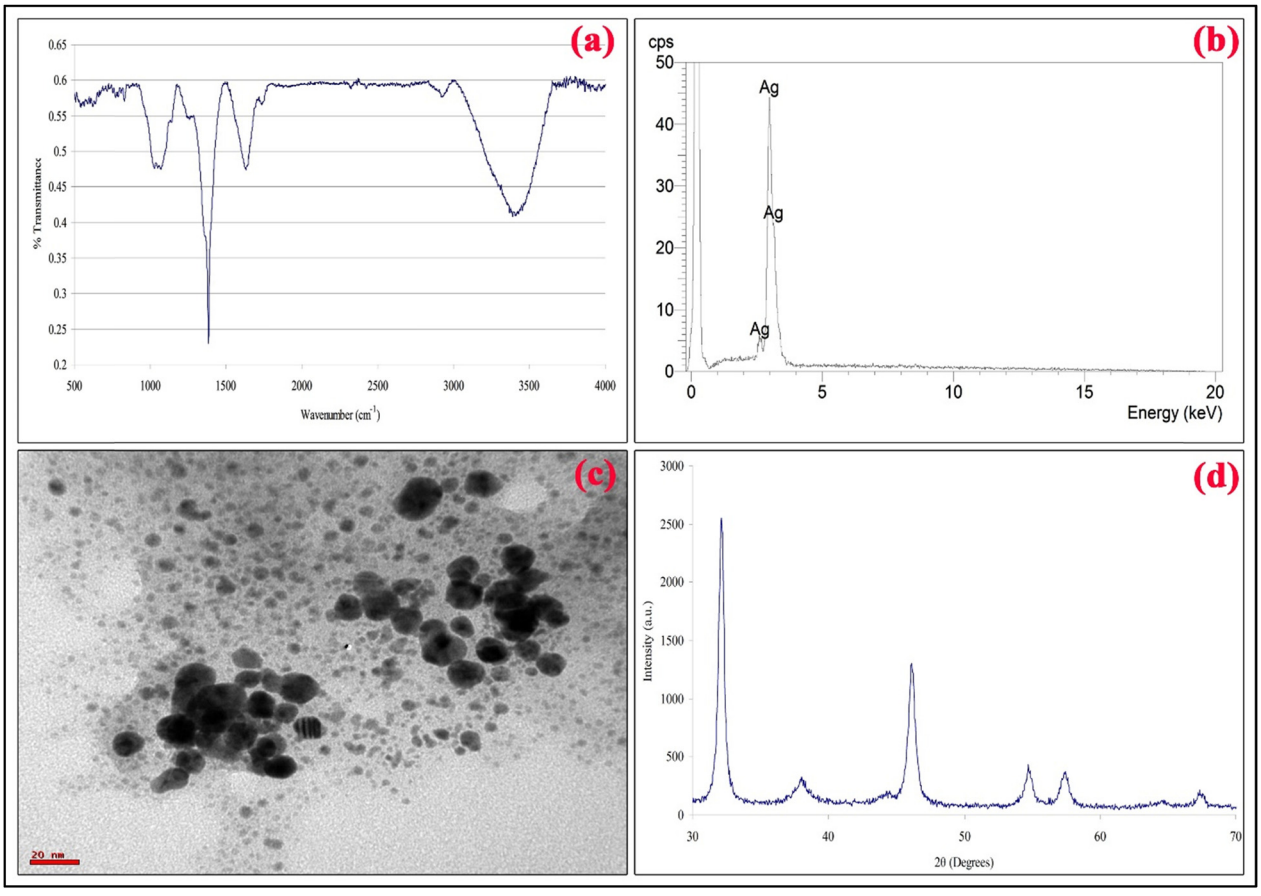

Figure 3: (a) FTIR absorption spectrum obtained from AgNPs by the reduction with $AgNO_3$ ions using the *C. alata* leaf extract. (b) XRD pattern of synthesized AgNPs using the *C. alata* leaf extract. (c) TEM images illustrating the formation of AgNPs (20 nm), synthesized using the *C. alata* leaf extract. (d) EDS spectrum of AgNPs with 1 mM $AgNO_3$.

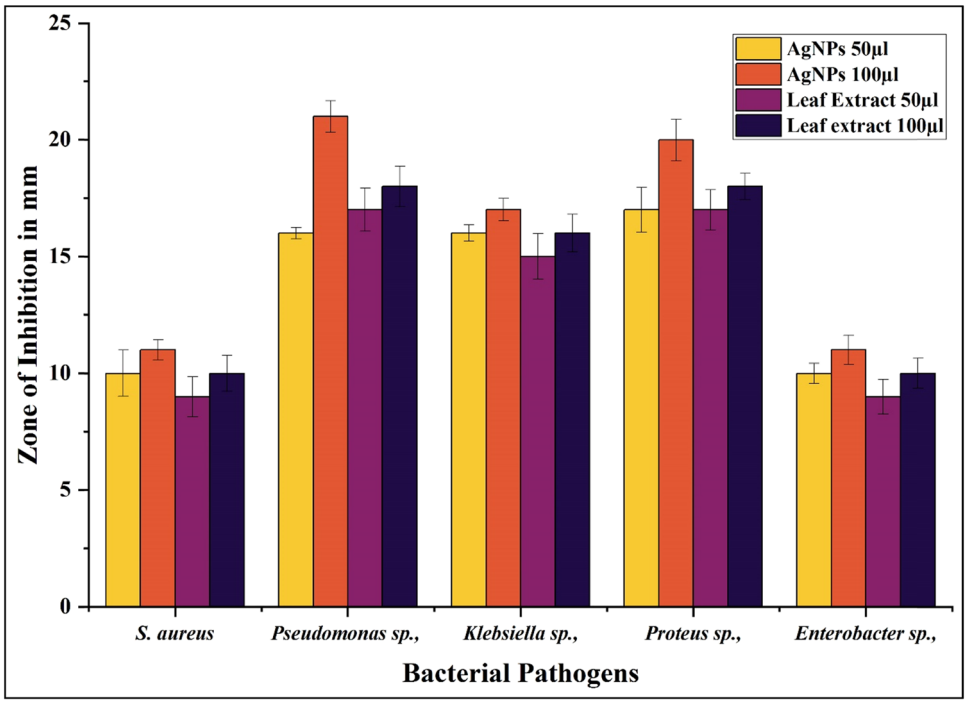

Figure 4: Antibacterial activity of the *C. alata* leaf extract and synthesized AgNPs.

3.3 Antibacterial activity

The efficacy of the synthesized AgNPs mediated by *C. alata* leaf extract against *S. aureus*, *Pseudomonas* sp., *Klebsiella* sp., *Proteus* sp., and *Enterobacter* sp. was examined. The resulting AgNPs' antibacterial efficacy was evaluated by measuring the diameter of the inhibitory zone. In comparison to other test strains, *S. aureus* (10 ± 0.98 mm) and *Enterobacter* sp. (10 ± 0.43 mm) showed minimal inhibition followed by *Klebsiella* sp. (16 ± 0.35 mm), *Pseudomonas* sp. (10 ± 0.24 mm), and *Proteus* sp. (17 ± 0.95 mm) at a minimum (50 µg·mL^{-1}) concentration level. A maximum zone of inhibition was obtained for *Pseudomonas* sp. (21 ± 0.67 mm), followed by *Proteus* sp. (20 ± 0.89 mm), *Klebsiella* sp. (17 ± 0.48 mm), *S. aureus* (11 ± 0.43 mm), and *Enterobacter* sp. (11 ± 0.62 mm) at a higher concentration (100 µg·mL^{-1}) (Figure 4). In this work, the microdilution method was used to assess the minimal inhibitory concentration (MIC) of AgNPs and leaf extract against tested pathogens and was found to be effective against a variety of organisms, and the positive control was tetracycline at 25 µg·mL^{-1} (Table 2).

Table 2: MIC of the *C. alata* leaf extract and synthesized AgNPs against bacterial pathogens

Pathogens	MIC (mg·mL^{-1})		Tetracycline (µg·mL^{-1})
	AgNPs	Leaf extract	
S. aureus	5.18	6.08	25
Pseudomonas sp.	3.16	4.25	25
Klebsiella sp.	4.26	5.89	25
Proteus sp.	4.16	5.32	25
Enterobacter sp.	6.86	7.43	25

With all the examined bacteria, the *C. alata* leaf extract showed a very small zone of inhibition. The silver nitrate act as an inhibiting growth agent for all tested bacteria. The zone of inhibition depends on the concentration of the AgNPs used. The adhesion of AgNPs to bacterial cell walls is often what causes their bactericidal activity [28]. As a result, this connection promotes the accumulation of the envelope protein precursor, which results in protein denaturation, proton motivation force reduction, and ultimately cell death. The antibacterial activity of NPs is significantly influenced by their size. The bacterial cell membranes can more readily absorb smaller nanoparticles. This is because tiny particles have more surface area for interacting with microbes and releasing Ag^{+} through oxidation. This quickens the production of reactive oxidant species, which further compromises the cellular structure and ultimately leads to cell death. Therefore, the AgNPs of the *C. alata* leaf extract have been able to enter the cell freely and cause harm due to their small size [29–31].

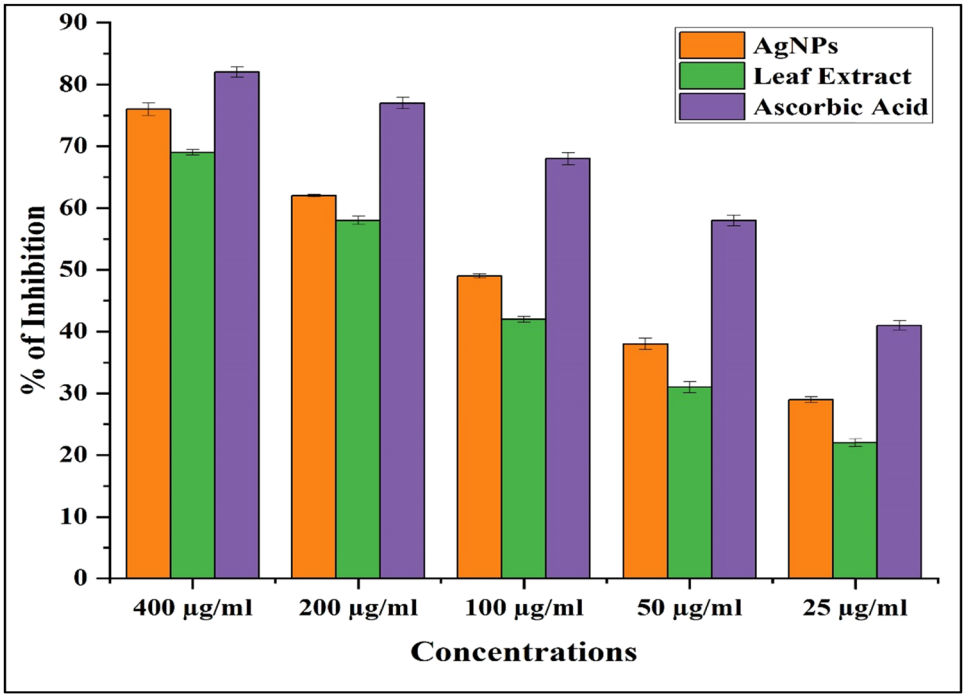

Figure 5: DPPH free radical scavenging activity of the *C. alata* leaf extract and synthesized AgNPs.

3.4 Antioxidant activity

Antioxidants are substances that scavenge free radicals and protect against diseases that cause degeneration, such as cancer, Parkinson's disease, Alzheimer's disease, and atherosclerosis, which are due to oxidative stress (excess production of free radicals) [20]. The role of phenolic compounds, such as phenolic acids and flavonoids,

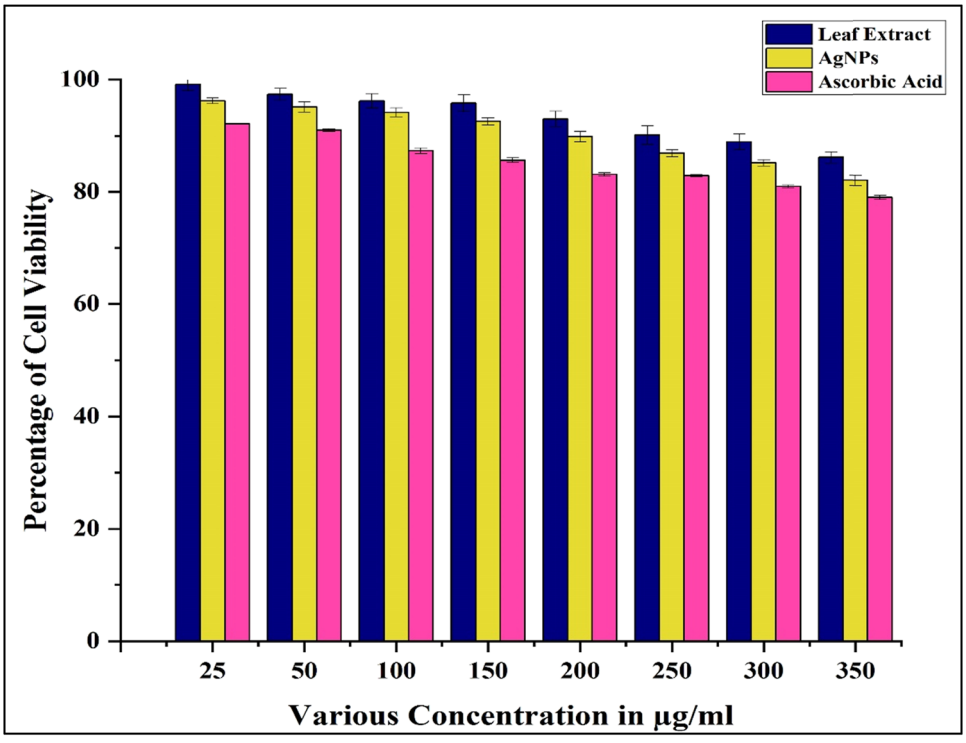

Figure 6: MTT assay using the lung cancer cell line A549.

present in medicinal plants is to give their hydrogen atom and scavenge free radicals (ROS) [32]. The findings of the current study showed that AgNPs have antioxidant properties at various concentrations (25–400 $\mu g \cdot mL^{-1}$) as determined using DPPH assay. The results demonstrated that the percentage inhibition increased as the concentrations of AgNPs, leaf extract, and ascorbic acid increased from 25 to 400 $\mu g \cdot mL^{-1}$ (Figure 5). Higher concentrations of AgNPs and ascorbic acid were used in the DPPH experiment to measure the antioxidant activity. The higher polyphenolic content of the leaf extract that is capped on AgNPs may be the reason for the improved antioxidant capacity [33].

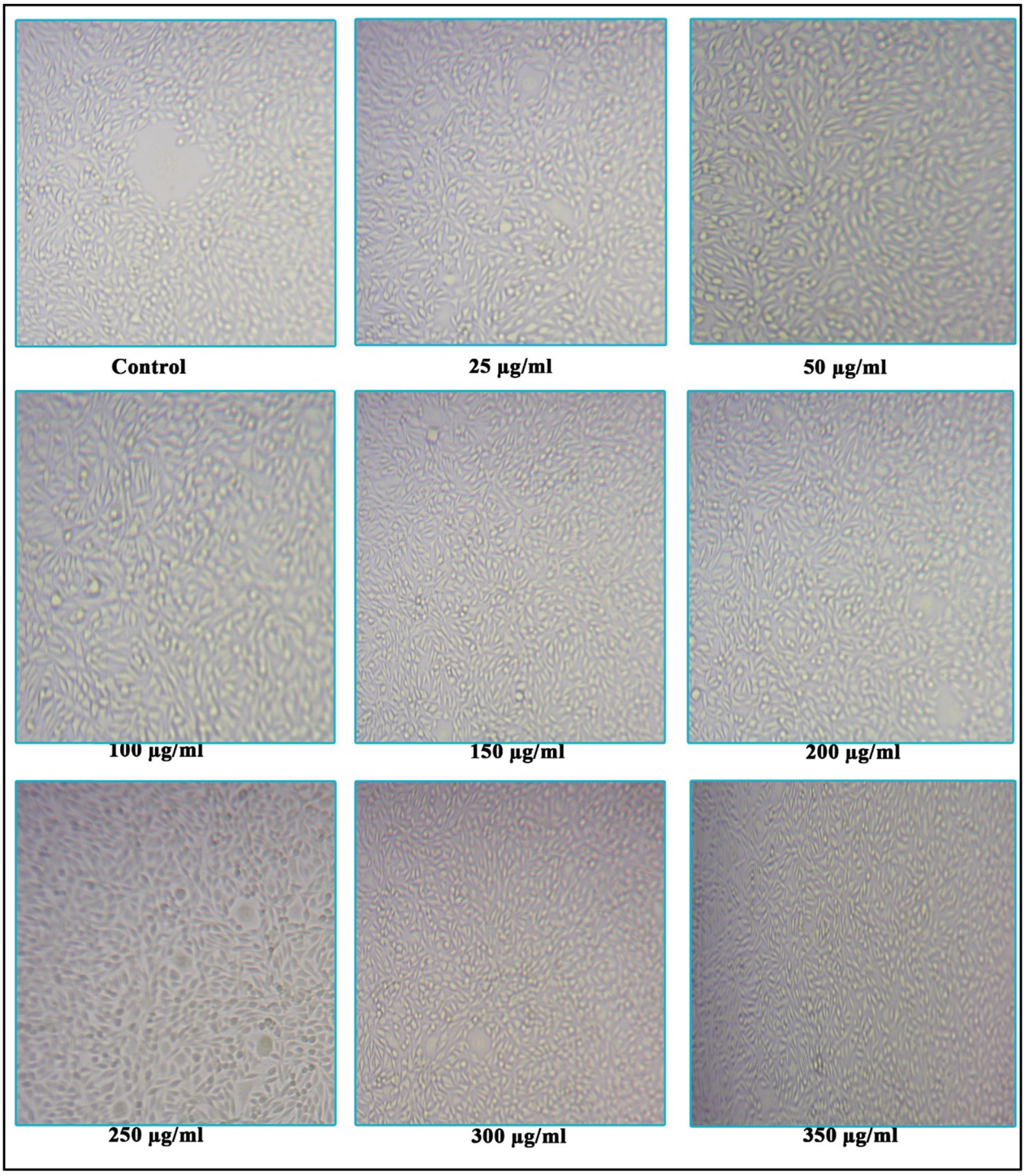

Figure 7: Microscopic images show morphological changes observed in the cells during the MTT assay.

By effectively reducing the reactive oxygen species, AgNPs showed a broad spectrum of antioxidant activity in each of these studies [34].

3.5 *In vitro* cytotoxicity

Using the A549 cell line, the cytotoxicity of the produced AgNPs was evaluated *in vitro*. For 24 h, several concentrations of AgNPs (ranging from 25 to 400 $\mu g \cdot mL^{-1}$) were applied to the cell line, and the results were compared to the control DMEM. The cellular oxidoreductase enzyme causes MTT and other chemicals to turn yellow based on the metabolic processes taking place inside the cell [35]. The cells' viability was drastically decreased, with an IC_{50} value of $50 \pm 4.9\ \mu g \cdot mL^{-1}$ and the positive control doxorubicin exhibits an IC_{50} value of $40 \pm 2.4\ \mu g \cdot mL^{-1}$. According to the cell line results, compared to other concentrations, the low concentration of AgNPs demonstrated 98% cell viability (Figure 6). High density was shown to have altered morphology due to the elevated cytotoxic effect (Figure 7).

4 Conclusion

The extract *of C. alata* aqueous leaves has been effectively used for the synthesis of AgNPs, and the efficacy of *C. alata* leaves was demonstrated as a natural, renewable, and low-cost bioreduction agent of silver and capping agents. Characterization of the synthesized nanoparticles using UV-visible, FTIR, TEM, EDX, and XRD studies revealed the formation of AgNPs and confirmed the functional groups of the extract; the mean size of AgNPs was found to be 13.54 nm, with a spherical shape as obtained from the cubic crystal structure, respectively. AgNPs demonstrated potent antibacterial activity against skin infections, demonstrating their medicinal significance. AgNPs are therefore crucial for the biomedical or pharmaceutical sector's production of antibacterial skin ointments. The photosynthesis of AgNPs raises the possibility of creating a medicinal formulation with antibacterial properties.

Acknowledgments: This work was supported by the National Research Foundation of Korea (NRF) grant, funded by the Korea Government (MSIT) (No. 2021054783). The authors extend their appreciation to the Researchers Supporting Project Number (RSP2023R143), King Saud University, Riyadh, Saudi Arabia.

Funding information: The project was funded by the Researchers Supporting Project Number (RSP2023R143), King Saud University, Riyadh, Saudi Arabia.

Author contributions: Kanagasabapathy Sivasubramanian: conceptualization, investigation, data collection, formal analysis, methodology, writing – original draft, and visualization; Shanmugam Sabarinathan and Moorthy Muruganandham: formal analysis and visualization; Abdulrahman I. Almansour: formal analysis and methodology; Natarajan Arumugam: formal analysis and, methodology; Palanivel Velmurugan and Subpiramaniyam Sivakumar: formal analysis, writing – review and editing; Raju Suresh Kumar: project administration, conceptualization, supervision, formal analysis, methodology, validation, writing – original draft, writing – review and editing, and visualization.

Conflict of interest: The authors state no conflict of interest.

References

[1] Loganathan S, Selvam K, Padmavathi G, Shivakumar MS, Senthil-Nathan S, Sumathi AG, et al. Biological synthesis and characterization of *Passiflora subpeltata* Ortega aqueous leaf extract in silver nanoparticles and their evaluation of antibacterial, antioxidant, anti-cancer and larvicidal activities. J King Saud University-Science. 2022;34(3):101846.

[2] Yin IX, Zhang J, Zhao IS, Mei ML, Li Q, Chu CH. The antibacterial mechanism of silver nanoparticles and its application in dentistry. Int J Nanomed. 2020;17:2555–62.

[3] Kędziora A, Wieczorek R, Speruda M, Matolínová I, Goszczyński TM, Litwin I, et al. Comparison of antibacterial mode of action of silver ions and silver nanoformulations with different physico-chemical properties: Experimental and computational studies. Front Microbiol. 2021;12:659614.

[4] Wulandari IO, Pebriatin BE, Valiana V, Hadisaputra S, Ananto AD, Sabarudin A. Green synthesis of silver nanoparticles coated by water soluble chitosan and its potency as non-alcoholic hand sanitizer formulation. Materials. 2022;15(13):4641.

[5] Rai MK, Deshmukh SD, Ingle AP, Gade AK. Silver nanoparticles: the powerful nanoweapon against multidrug-resistant bacteria. J Appl Microbiology. 2012;112(5):841–52.

[6] Singh R, Singh D. Chitin membranes containing silver nanoparticles for wound dressing application. Int Wound J. 2014;11(3):264–8.

[7] Xu L, Yi-Yi W, Huang J, Chun-Yuan C, Zhen-Xing W, Xie H. Silver nanoparticles: Synthesis, medical applications and biosafety. Theranostics. 2020;10(20):8996.

[8] Herrero-Calvillo R, Landeros-Páramo L, Santos-Ramos I, Rosas G. AgNPs/AgCl cube-shaped particles synthesized by a

green method and their catalytic application. J Clust Sci. 2022;8:1–9.
[9] Boateng J, editor. Therapeutic dressings and wound healing applications. Vol. 9. New York: John Wiley & Sons; 2020.
[10] Yon JA, Lee SK, Keng JW, Chow SC, Liew KB, Teo SS, et al. Cassia alata (Linnaeus) roxburgh for skin: Natural remedies for atopic dermatitis in Asia and their pharmacological activities. Cosmetics. 2022;10(1):5.
[11] Chua LY, Chua BL, Figiel A, Chong CH, Wojdyło A, Szumny A, et al. Characterisation of the convective hot-air drying and vacuum microwave drying of *Cassia alata*: Antioxidant activity, essential oil volatile composition and quality studies. Molecules. 2019;24(8):1625.
[12] Fatmawati S, Purnomo AS, Bakar MF. Chemical constituents, usage and pharmacological activity of *Cassia alata*. Heliyon. 2020;6(7):04396.
[13] Jayasree R, Prathiba R, Sangavi S. Immunomodulatory effect of *Cassia alata* petals in Garra rufa (doctor fish). J Chem Pharm Sci. 2016;9(1):215–8.
[14] Netala VR, Kotakadi VS, Domdi L, Gaddam SA, Bobbu P, Venkata SK, et al. Biogenic silver nanoparticles: efficient and effective antifungal agents. Appl Nanosci. 2016;6:475–84.
[15] Manikandan V, Velmurugan P, Park JH, Chang WS, Park YJ, Jayanthi P, et al. Green synthesis of silver oxide nanoparticles and its antibacterial activity against dental pathogens. 3 Biotech. 2017;7:1–9.
[16] Boulc'h F, Schouler MC, Donnadieu P, Chaix JM, Djurado E. Domain size distribution of Y-TZP nano-particles using XRD and HRTEM. Image Anal Stereol. 2001;20(3):157–61.
[17] Kharissova OV, Dias HR, Kharisov BI, Pérez BO, Pérez VM. The greener synthesis of nanoparticles. Trends Biotechnol. 2013;31(4):240–8.
[18] Krishnaraj C, Jagan EG, Rajasekar S, Selvakumar P, Kalaichelvan PT, Mohan NJ. Synthesis of silver nanoparticles using *Acalypha indica* leaf extracts and its antibacterial activity against water borne pathogens. Colloids Surf B: Biointerfaces. 2010;76(1):50–6.
[19] Lal S, Verma R, Chauhan A, Dhatwalia J, Guleria I, Ghotekar S, et al. Antioxidant, antimicrobial, and photocatalytic activity of green synthesized ZnO-NPs from *Myrica esculenta* fruits extract. Inorg Chem Commun. 2022;141:109518.
[20] Wei W, Wang L, Xu L, Zeng J. Anticancer mechanism of brevis-capine in non-small cell lung cancer A549 cells acts via ROS-mediated upregulation of IGFBP4. J Thorac Dis. 2021;13(4):2475.
[21] Balashanmugam P, Kalaichelvan PT. Biosynthesis characterization of silver nanoparticles using *Cassia roxburghii* DC. aqueous extract, and coated on cotton cloth for effective antibacterial activity. Int J Nanomed. 2015;10(2):87–97.
[22] Meshram SM, Bonde SR, Gupta IR, Gade AK, Rai MK. Green synthesis of silver nanoparticles using white sugar. IET Nanobiotechnol. 2013;7(1):28–32.
[23] Pettegrew C, Dong Z, Muhi MZ, Pease S, Mottaleb MA, Islam MR. Silver nanoparticle synthesis using monosaccharides and their growth inhibitory activity against gram-negative and positive bacteria. Int Sch Res Not. 2014;2014:1–8.
[24] Vijayakumari A, Sinthiya A. Biosynthesis of phytochemicals coated silver nanoparticles using aqueous extract of leaves of *Cassia alata* – characterization, antibacterial and antioxidant activities. Int J Pharm Clin Res. 2018;10(5):138–49.
[25] Murugan R, Parimelazhagan T. Comparative evaluation of different extraction methods for antioxidant and anti-inflammatory properties from *Osbeckia parvifolia* Arn.–An *in vitro* approach. J King Saud Univ-Sci. 2014;26(4):267–75.
[26] Prakash P, Gnanaprakasam P, Emmanuel R, Arokiyaraj S, Saravanan M. Green synthesis of silver nanoparticles from leaf extract of *Mimusops elengi*, Linn. for enhanced antibacterial activity against multi drug resistant clinical isolates. Colloids Surf B: Biointerfaces. 2013;108:255–9.
[27] Singh K, Panghal M, Kadyan S, Chaudhary U, Yadav JP. Antibacterial activity of synthesized silver nanoparticles from *Tinospora cordifolia* against multi drug resistant strains of *Pseudomonas aeruginosa* isolated from burn patients. J Nanomed Nanotechnol. 2014;5(2):1.
[28] Singh S, Singh SK, Yadav A. A review on *Cassia* species: Pharmacological, traditional and medicinal aspects in various countries. Am J Phytomed Clin Ther. 2013;1(3):291–312.
[29] Guan Z, Ying S, Ofoegbu PC, Clubb P, Rico C, He F, et al. Green synthesis of nanoparticles: Current developments and limitations. Environ Technol Innov. 2022;102336.
[30] Vanlalveni C, Lallianrawna S, Biswas A, Selvaraj M, Changmai B, Rokhum SL. Green synthesis of silver nanoparticles using plant extracts and their antimicrobial activities: A review of recent literature. RSC Adv. 2021;11(5):2804–37.
[31] Tarhan L, Urek RO, Oner A, Nakiboglu M. Evaluation of phenolic profiles, antioxidant activities, and cytotoxic and apoptotic potentials of *Phlomis angustissima* and *Phlomis fruticosa*, medicinal plants from Turkey. Eur J Integr Med. 2022;55:102188.
[32] Labulo AH, David OA, Terna AD. Green synthesis and characterization of silver nanoparticles using *Morinda lucida* leaf extract and evaluation of its antioxidant and antimicrobial activity. Chem Pap. 2022;16:1–3.
[33] Moorthy K, Chang KC, Yu PJ, Wu WJ, Liao MY, Huang HC, et al. Synergistic actions of phytonutrient capped nanosilver as a novel broad-spectrum antimicrobial agent: unveiling the antibacterial effectiveness and bactericidal mechanism. N J Chem. 2022;46(32):15301–12.
[34] Berridge MV, Herst PM, Tan AS. Tetrazolium dyes as tools in cell biology: new insights into their cellular reduction. Biotechnol Annu Rev. 2005;11:127–52.